Influence of Osteon Area Fraction and Degree of Orientation of HAp Crystals on Mechanical Properties in Bovine Femur

Satoshi YAMADA[a], Shigeru TADANO[a,*], Kazuhiro FUJISAKI[a], and Yuka KODAKI

[a] Division of Human Mechanical Systems and Design, Faculty of Engineering, Hokkaido University, N13 W8, Kita-ku, Sapporo, Hokkaido 060-8628, Japan
[b] Division of Human Mechanical Systems and Design, Graduate School of Engineering, Hokkaido University, N13 W8, Kita-ku, Sapporo, Hokkaido 060-8628, Japan

*Corresponding Author:
Shigeru TADANO, PhD
Professor, Division of Human Mechanical Systems and Design, Faculty of Engineering, Hokkaido University
N13 W8, Kita-ku, Sapporo, Hokkaido 060-8628, Japan
Tel/Fax: +81-11-7066405
E-mail: tadano@eng.hokudai.ac.jp

Word count: 2908 words (Introduction through Acknowledgement)
Manuscript Type: Original Article
Keywords: Biomechanics, Bone, Osteon, Hydroxyapatite, X-ray Diffraction

Abstract

Cortical bone has a hierarchical structure, spanning from the macrostructure at several millimeters or whole bone level, the microstructure at several hundred micrometers level, to the nanostructure at hydroxyapatite (HAp) crystals and collagen fibrils levels. The aim of the study is to understand the relationship between the HAp crystal orientation and the elastic modulus and the relationship between the osteon area fraction and the deformation behavior of HAp crystals in cortical bone. In the experiments, five strip specimens (40×2×1 mm) aligned with the bone axis were taken from the cortical bone of a bovine femur. The degree of *c*-axis orientation of HAp crystals in the specimens was measured with X-ray diffraction technique with the imaging plate. To measure the deformation behavior of HAp crystals in the specimens, tensile tests under X-ray irradiation were conducted. The specimens were cut at the X-ray measurement positions and osteon area fraction and porosity at the transverse cross-sections were observed. Further, the volume fraction of HAp of the specimens was measured. Results showed the degree of *c*-axis orientation of HAp crystals was positively correlated with the elastic modulus of the specimens (r = 0.94). The volume fraction of HAp and the porosity showed no statistical correlation with the elastic modulus and the tensile strength. The HAp crystal strain ε^H increased linearly with the

bone tissue strain ε. The average value of $\varepsilon^H/\varepsilon$ was 0.69 ± 0.13 and there was no correlation between the osteon area fraction and $\varepsilon^H/\varepsilon$ (r = -0.27, p = 0.33). The results suggest that the degree of *c*-axis orientation of HAp crystals affects the elastic modulus and the magnitude of HAp crystal strain does not depend on the osteon area fraction. (280 words)

1. Introduction

The mechanical properties and the stress/strain of cortical bone are very important in order to evaluate the risk of bone fracture, the progress of bone healing, and the stage of bone disease (i.e. osteoporosis). As shown in Fig. 1, cortical bone has a hierarchical structure, spanning from the macrostructure at several millimeters or whole bone level, the microstructure at several hundred micrometers level, including osteons and Haversian canals, to the nanostructure at hydroxyapatite (HAp) crystals and collagen fibrils level. The macroscopic mechanical properties are closely related with the hierarchical properties of cortical bone, and the measurement of the macroscopic stress/strain may require consideration of the hierarchical properties.

In the microstructure, osteons consist of lamellae, thin plate-like structures, surrounding a cylindrical Haversian canal, and are nearly 300-400 micrometers in diameter. The osteons in many cases are aligned along the bone axis, that is the longitudinal axis of the bone, although some bones' osteons are not aligned with the axis (Britz et al., 2012; Hert et al., 1994). Here, the cortical bone is regarded as a composite of the osteonal region formed by lamellas and the non-osteonal regions (Fig. 1). In the nanostructure, the cortical bone is composed of HAp and collagen matrix. The HAp has a hexagonal crystal structure, and the *c*-axis of the HAp crystals in cortical

bone is typically aligned with the bone axis.

Various studies have been conducted on the multi-scale mechanical characterization in cortical bone (Hoffler et al., 2000; Rho et al., 2002; Gibson et al., 2006; Gupta et al., 2006; Hoc et al., 2006; Wang et al., 2006; Almer and Stock, 2007; Akhtar et al., 2008; Feng and Jasiuk, 2011; Tadano and Giri, 2011). For instance, it was reported that the elastic modulus in osteonal bone was lower than that in interstitial bone (Rho et al., 2002) and the elastic modulus of the tissue in the bone axis decreased with the osteon area fraction in the cross-sections of specimens (Gibson et al., 2006). However, although it is known that bone mineral density affects the macroscopic mechanical properties of bone, the nanostructural effects on the macroscopic mechanical properties of bone have not been fully investigated and elucidated. X-ray diffraction is a promising tool to characterize the bone nanocomposites (Tadano and Giri, 2011). Previous reports indicated site-specific HAp crystal orientation in cortical bone using X-ray diffraction techniques (Giri et al., 2008; Tadano and Giri, 2011). The influence of the HAp crystal orientation on the mechanical properties of cortical bone has not been elucidated yet. Further, the authors have also reported the deformation behavior of HAp crystals in cortical bone measured by X-ray diffraction techniques in order to measure the macroscopic stress/strain from the HAp crystal deformation

(Fujisaki et al., 2006; Fujisaki and Tadano, 2007; Tadano et al., 2008; Giri et al., 2009; Tadano and Giri, 2011) and the presence of residual stresses in cortical bone measured from the crystal deformation (Yamada and Tadano, 2010; Yamada et al., 2011; Tadano and Giri, 2011). In these measurements, the influence of the microstructure on the macroscopic stress/strain estimation of cortical bone has not been discussed. The influence of osteon area fraction and degree of orientation of HAp crystals on the mechanical properties explained with elastic modulus, strength, and magnitude of HAp crystal deformation have not been fully investigated and elucidated.

The current study hypothesized that the HAp crystal orientation and bone mineral density would independently affect the macroscopic mechanical properties of bone and that the osteon area fraction would also affect the mechanical properties dependently of these nanostructural effects. The study investigated the relationship between the osteon area fraction and the elastic modulus, the relationship between the HAp crystal orientation and the elastic modulus, and the relationship between the osteon area fraction and the deformation behavior of HAp crystals using bovine cortical bone specimens. Further, the volume fraction of HAp and the porosity of the specimens were also measured.

2. Materials and Methods

Specimen

Five strip specimens of 40×2×1 mm were cut from the cortical bone of the middle diaphysis of an adult bovine femur (24-month-old) with a low speed diamond wheel saw (Model 650, South Bay Technology, USA), and the longitudinal direction of the specimens was aligned with the bone axis. A strain gauge (KFG-1N-120-C1-11L3M3R, KYOWA, Japan) was glued to the surface of the specimens for the measurements of the tissue strain (Fig. 2). To stretch these specimens with a small tensile test device, thin metal jigs were glued to both ends of the specimens. The specimens were air dried and then the measurements were conducted. The measurement positions in each specimen were at three points.

HAp crystal strain in tensile test

When bone tissue is irradiated with X-rays, the X-rays diffract in the lattice planes of the HAp crystals, which have a hexagonal crystal structure, satisfying Eq. (1).

$$2d\sin\theta = n\lambda \quad (1)$$

Equation (1) relates the Bragg angle θ to the interplanar spacing d at a lattice plane using characteristic X-rays with a unique wavelength λ. The HAp crystal strain ε^{H} was

obtained from the displacement of the interplanar spacing of the lattice plane as in Eq. (2), where d_0 is the interplanar spacing and θ_0 is the Bragg angle at the non-strained condition.

$$\varepsilon^H = \frac{d - d_0}{d_0} = \frac{\sin\theta_0 - \sin\theta}{\sin\theta} \tag{2}$$

In the study, the specimens were irradiated with X-rays in the tensile tests, as suggested in Fig. 2(a). An X-ray diffractometer (Ultima IV, Rigaku, Japan) was used with characteristic X-rays of Mo-Kα (λ ~ 0.071 nm), tube voltage 40 kV, and tube current 40 mA, using a 1 mm in diameter collimator. The X-ray diffraction profiles were measured by a scintillation counter between 2θ = 11.0 deg and 12.5 deg, which includes the diffraction angle of the (002) plane of HAp crystals. The Bragg angle of the plane in Eq. (2) was defined as half of the angle at the peak position of the X-ray diffraction profile, and the peak position was determined by applying the full width at two-thirds maximum (FWTTM) method (Yamada et al., 2011). The HAp crystal strain ε^H was measured three times at each tissue strain condition (ε = 0, 500 μ, 1000 μ, 1500 μ, and 2000 μ) with the small tensile test device attached to the X-ray diffractometer.

Degree of orientation of HAp crystals

The *c*-axis of the HAp crystals in cortical bone tends to be aligned with the

bone axis. The current study focused on the degree of *c*-axis orientation of the crystals in the bone axis.

As shown in Fig. 2(b), the specimen in the non-strained condition was irradiated for 10 minutes with the X-rays. The traveling direction and the intensity of the diffracted X-rays depend on the direction and the number of the lattice planes, respectively. The X-ray diffraction pattern of each specimen was detected by an X-ray Imaging Plate (IP) (BAS-SR 127×127 mm, FUJIFILM, Japan) and read with a scanner (R-axis DS3C, Rigaku, Japan). The X-ray diffraction pattern of the (002) planes of HAp crystals appears as arcs, because the (002) plane is perpendicular to the *c*-axis oriented to the bone axis. In this study, the degree of *c*-axis orientation of the crystals is defined as in Eq. (3) using the X-ray diffraction pattern of the (002) planes (Giri et al., 2009; Tadano and Giri, 2011).

$$< \cos^2 \beta >= \frac{\int_{-\pi/2}^{\pi/2} I(\beta) \cos^2 \beta |\sin \beta| d\beta}{\int_{-\pi/2}^{\pi/2} I(\beta) |\sin \beta| d\beta} \tag{3}$$

$I(\beta)$ is the diffracted intensity at the azimuth angle β in the X-ray diffraction pattern of the lattice plane. If the *c*-axis is completely oriented in the bone axis, the $<\cos^2\beta>$ is equal to 1.

Measurement of elastic modulus and tensile strength

After the X-ray measurements, tensile tests were conducted with a material testing machine (Model 4411: INSTRON, USA) to measure the elastic modulus and tensile strength of the specimens as the mechanical properties of tissue level.

Osteon area fraction and porosity in the cross-section

After the tensile tests, the specimens were embedded in epoxy resin for 24 hours and cut at the X-ray measurement positions by the diamond wheel saw. The transverse cross-sections were ground by emery papers (up to #2000) and buffed by a buffing machine (Model 900: South Bay Technology, USA). Then, the cross-section was observed by an optical microscope (VH5000: KEYENCE, Japan), as shown in Fig. 3. The study measured the osteon area fraction (OA) defined as the area fraction of osteonal region with respect to the total area of cross-section and the porosity defined as the area fraction of blood vessel area with respect to the total area as in Eq. (4) and (5).

$$OA = \frac{\text{(Osteonal region) - (Blood vessel area)}}{\text{(Total area) - (Blood vessel area)}} \tag{4}$$

$$Porosity = \frac{\text{(Blood vessel area)}}{\text{(Total area)}} \tag{5}$$

Further, $\overline{OA}$ and $\overline{Porosity}$ were defined as the average of OA and $Porosity$ at three measurement positions in each of the five specimens, respectively.

Volume fraction of HAp

To determine the volume fraction of HAp v_{HAp} of the specimens, the X-ray absorption experiments were conducted using the previous method (Todoh et al., 2009). The specimens were sliced into 0.9 mm thick plate at the points of the observed cross-sections. The sliced specimens were irradiated with X-rays and the v_{HAp} was quantified by the transmitted X-ray intensity.

3. Results

Macrostructure vs. Microstructure

The *OA* varied greatly between measurement positions in the five specimens, from 0.13 to 0.63, with the average ratio 0.48 ± 0.13. However, the differences in individual specimens were small. The average of the standard deviations in each specimen was 0.04, and *OA* did not depend on the longitudinal position in the specimen.

Figure 4(a) shows the relationship between the elastic modulus in the bone axis and $\overline{OA}$. The elastic modulus had a strong negative correlation with $\overline{OA}$ (r = -0.96, p < 0.05). Figure 4(b) shows the relationship between the tensile strength and $\overline{OA}$. The tensile strength was higher in specimens with smaller osteonal area (r = -0.94, p < 0.05).

The average value of $\overline{Porosity}$ was 0.08 ± 0.01 and did not vary much in the

specimens used in the study. The $\overline{Porosity}$ had no statistical correlation with the elastic modulus (r = -0.80, p = 0.10) and the tensile strength (r = -0.84, p = 0.07), however, *Porosity* had a positive correlation with *OA* (r = 0.75, p < 0.01).

Microstructure vs. Nanostructure

Figure 5 shows the deformation behavior of the HAp crystals. The horizontal axis indicates the applied tissue strain ε and the vertical axis is the HAp crystal strain ε^H calculated with Eq. (2). The HAp crystal strain increased linearly with the bone tissue strain (the value of R^2 was 0.95 in Fig. 5). The study calculated the value of $\varepsilon^H/\varepsilon$ by the linear least-squares method at each measurement position. The average of $\varepsilon^H/\varepsilon$ among the five specimens was 0.69 ± 0.13, and $\varepsilon^H/\varepsilon$ had no statistical correlation with *OA* (r = -0.27, p = 0.33) and *Porosity* (r = -0.13, p = 0.64).

Figure 6 shows the relationship between the degree of *c*-axis orientation of the HAp crystals $\langle\cos^2\beta\rangle$ and *OA*. Although there was no large difference in the values of $\langle\cos^2\beta\rangle$ among the five specimens ($\langle\cos^2\beta\rangle$ = 0.374 ± 0.007), the value of $\langle\cos^2\beta\rangle$ was strongly negatively correlated with *OA* (r = -0.90, p < 0.01). Further, v_{HAp} had a negative correlation with *OA* (r = -0.84, p < 0.01). The average value of v_{HAp} was 0.60 ± 0.03 and did not vary much.

Macrostructure vs. Nanostructure

The v_{HAp} had no statistical correlation with the elastic modulus (r = 0.56, p = 0.33) and the tensile strength (r = 0.39, p = 0.52).

Figure 7 indicates the relationship between the elastic modulus and the average of the values of $\langle\cos^2\beta\rangle$. The $\langle\cos^2\beta\rangle$ value was strongly positively correlated with the elastic modulus (r = 0.94, $p < 0.05$). The c-axis of the HAp crystals is more closely aligned with the bone axis in specimens with higher elasticity. Further, the $\langle\cos^2\beta\rangle$ value was also strongly positively correlated with the tensile strength (r = 0.90, $p < 0.05$).

4. Discussion

The *OA* varied greatly between the five specimens, but *OA* did not depend on the longitudinal position in the specimens. Figure 8 suggests the three-dimensional architecture of osteons in cortical bone. It was confirmed that although some osteons bifurcated and converged, osteons were generally aligned with the bone axis in the mid-diaphysis of bovine femur. Based on this, it may be considered that local mechanical properties also do not vary along the bone axis in a specimen.

Previous studies showed that the elastic modulus of osteonal bone was lower than that of interstitial bone and the elastic modulus related with the osteon area fraction (Rho et al., 1999; Rho et al., 2001; Rho et al., 2002; Gibson et al., 2006). The current study also indicated that the elastic modulus and the tensile strength were negatively correlated with *OA*. The mechanical properties at the macrostructure closely depend on the microstructure explained with osteon area fraction in cortical bone.

It is well known that bone mineral density affects the elasticity and the strength of the bone. In the current study, v_{HAp} showed no statistical correlation with the elastic modulus and the tensile strength of the specimens. Further, the porosity also showed no statistical correlation with these mechanical properties. It can be presumed that the smaller variations of bone mineral density and porosity than the elastic modulus and strength mean the existence of other factors to determine the mechanical properties of bone tissue.

There was strongly positively correlated between the elastic modulus and the degree of *c*-axis orientation of HAp crystals. This suggests that the elastic modulus of HAp crystals in the *c*-axis is higher than that in the other axes, and the elastic modulus in the macrostructure depends on the *c*-axis orientation of HAp crystals. Although there may be effects of drying the specimens on the value of mechanical properties, the

drying process was the same for all specimens and the strong correlation may not be affected in the study. The results suggest the possibility of the less invasive estimation of macroscopic mechanical properties using the crystal orientation measured by the X-ray diffraction technique together with bone mineral density by X-ray absorption method. The limitation of this study was the use of five specimens from a bovine femur. However, to minimize the variability of bone mineral density and to distinguish the relationship between the HAp crystal orientation and the mechanical properties, the specimens from a bovine femur were used in this study. Although the sample size may be enough to show the applicability of the techniques, future studies will be conducted by increasing the sample size to elucidate further the current findings.

The degree of *c*-axis orientation of HAp crystals negatively correlated with the *OA*. The *c*-axis of the HAp crystals was more closely aligned with the bone axis in specimens with smaller osteonal area. This suggests that the degree of *c*-axis orientation of HAp crystals in the osteonal region is lower than that in the non-osteonal region. Further, v_{HAp} had a negative correlation with *OA*. The results may explain the differences in the elastic modulus of the osteonal and non-osteonal regions. An osteon can be composed of several arrays of parallel collagen fibrils (Giraud-Guille, 1988; Weiner et al., 1997). The *c*-axis of HAp crystals in the osteonal region might closely

align with the collagen fibrils. Some previous studies reported that the predominant collagen fiber orientation (CFO) and the *c*-axis of HAp crystals were generally co-linear (Reisinger et al., 2011; Fratzl et al., 2004; Wagermaier et al., 2006). Skedros et al. (2006) showed that the predominant CFO and the *c*-axis of HAp crystals were not co-linear in bones subjected to simple in vivo loadings. The differences might depend on the regional differences in the osteon morphotypes explained by Skedros et al. (2009) and Martin et al. (1996). Since the bovine femur may be subjected to relatively complex in vivo loadings, the regional differences would not be present (Skedros et al., 2009; Skedros et al., 2011). The current study has not yet established the specific osteon morphotypes in the specimens. Other osteon morphotypes in bones subjected to more simple loadings might lead to different results.

There was also no correlation between the HAp deformation behavior explained with the value of $\varepsilon^H/\varepsilon$ and OA. The deformation of HAp crystals averaged at the X-ray irradiation area did not depend on the characteristics of the microstructure. This suggests the validity of the tissue strain measurements from the HAp crystal strain without needing information of the osteon area fraction. In the study, the macroscopic applied stress in the bone axis was expressed in Eq. (6), using the crystal strain and the degree of *c*-axis orientation of HAp crystals.

$$\sigma = E \cdot \varepsilon = (787 < \cos^2 \beta > -269) \cdot \frac{1}{0.693} \varepsilon^H \qquad (6)$$

This study used strip specimens taken from a bovine cortical bone with the tensile tests were carried out with X-ray irradiation, and the results of the study showed the influence of the microstructure expressed with the osteon area fraction on the mechanical properties of macrostructure and nanostructure. However, the effects of differences in the individual osteons (e.g. differences in morphotypes, three-dimensional architecture, and size) were not evaluated in the study. Nyman et al. (2006) made 200-250 μm diameter cylindrical bone specimens from the osteonal region of human cortical bone, and measured the concentration of collagen crosslinks in the micro specimens. To better understand the mechanical properties and crystal structure in the osteonal/non-osteonal regions, further study of the effects of these and other possible differences between individual osteons will need to be focused on the three-dimensional architecture of osteons or conducted with micro specimens especially developed to further elucidate this.

Acknowledgement

This work was supported by Grant-in-Aid for Scientific Research (A), MEXT (No. 19200035) and Grant-in-Aid for JSPS Fellows (No. 09J00736).

Conflict of interest statement

No actual or potential conflicts of interest exist.

References

Almer, J.D., Stock, S.R., 2007. Micromechanical response of mineral and collagen phases in bone. Journal of Structural Biology 157, 365-370.

Akhtar, R., Daymond, M.R., Almer, J.D., Mummery, P.M., 2008. Load transfer in bovine plexiform bone determined by synchrotron x-ray diffraction. Journal of Materials Research 23, 543-550.

Britz, H.M., Jokihaara, J., Leppänen, O.V., Järvinen, T.L.N., Cooper, D.M.L., 2012. The effects of immobilization on vascular canal orientation in rat cortical bone. Journal of Anatomy 220, 67-76.

Feng, L., Jasiuk, I., 2011. Multi-scale characterization of swine femoral cortical bone. Journal of Biomechanics 44, 313-320.

Fratzl, P., Gupta, H.S., Paschalis, E.P., Roschger, P., 2004. Structure and mechanical quality of the collagen–mineral nano-composite in bone. Journal of Materials Chemistry 14, 2115-2123.

Fujisaki, K., Tadano, S., Sasaki, N., 2006. A method on strain measurement of HAp in cortical bone from diffusive profile of X-ray diffraction. Journal of Biomechanics 39, 579-586.

Fujisaki, K., Tadano, S., 2007. Relationship between bone tissue strain and lattice strain of HAp crystals in bovine cortical bone under tensile loading. Journal of Biomechanics 40, 1832-1838.

Gibson, V.A., Stover, S.M., Gibeling, J.C., Hazelwood, S.J., Martin, R.B., 2006. Osteonal effects on elastic modulus and fatigue life in equine bone. Journal of Biomechanics 39, 217-225.

Giraud-Guille, M.M., 1988. Twisted plywood architecture of collagen fibrils in human compact bone osteons. Calcified Tissue International 42, 167-180.

Giri, B., Tadano, S., Fujisaki, K., Todoh, M., 2008. Understanding site-specific residual strain and architecture in bovine cortical bone. Journal of Biomechanics 41, 3107–3115.

Giri, B., Tadano, S., Fujisaki, K., Sasaki, N., 2009. Deformation of mineral crystals in cortical bone depending on structural anisotropy. Bone 44, 1111-1120.

Gupta, H.S., Seto, J., Wagermaier, W., Zaslansky, P., Boesecke, P., Fratzl, P., 2006. Cooperative deformation of mineral and collagen in bone at the nanoscale. PNAS 103, 17741-17746.

Hert J, Fiala P, Petrtýl M., 1994. Osteon orientation of the diaphysis of the long bones in man. Bone 15, 269-277.

Hoc, T., Henry, L., Verdier, M., Aubry, D., Sedel, L., Meunier, A., 2006. Effect of microstructure on the mechanical properties of Haversian cortical bone. Bone 38 466-474.

Hoffler, C.E., Moore, K.E., Kozloff, K., Zysset, P.K., Brown, M.B., Goldstein, S.A., 2000. Heterogeneity of bone lamellar-level elastic moduli. Bone 26, 603-609.

Martin, R.B., Gibson, V.A., Stover, S.M., Gibeling, J.C., Griffin, L.V., 1996. Osteon structure in the equine third metacarpus. Bone 19, 165-171.

Nyman, J.S., Roy, A., Acuna, R.L., Gayle, H.J., Reyes, M.J., Tyler, J.H., Dean, D.D., Wang, X., 2006. Age-related effect on the concentration of collagen crosslinks in human osteonal and interstitial bone tissue. Bone 39, 1210-1217.

Reisinger, A.G., Pahr, D.H., Zysset, P.K., 2011. Principal stiffness orientation and degree of anisotropy of human osteons based on nanoindentation in three distinct planes. Journal of the Mechanical Behavior of Biomedical Materials 4, 2113-2127.

Rho, J.Y., Zioupos, P., Currey, J.D., Pharr, G.M., 1999. Variations in the individual thick lamellar properties within osteons by nanoindentation. Bone 25, 295-300.

Rho, J.Y., Currey, J.D., Zioupos, P., Pharr, G.M., 2001. The anisotropic Young's modulus

of equine secondary osteones and interstitial bone determined by nanoindentation. Journal of Experimental Biology 204, 1775-1781.

Rho, J.Y., Zioupos, P., Currey J.D., Pharr, G.M., 2002. Microstructural elasticity and regional heterogeneity in human femoral bone of various ages examined by nano-indentation. Journal of Biomechanics 35, 189-198.

Skedros, J.G., Sorenson, S.M., Takano, Y., Turner, C.H., 2006. Dissociation of mineral and collagen orientations may differentially adapt compact bone for regional loading environments: results from acoustic velocity measurements in deer calcanei. Bone 39, 143-151.

Skedros, J.G., Mendenhall, S.D., Kiser, C.J., Winet, H., 2009. Interpreting cortical bone adaptation and load history by quantifying osteon morphotypes in circularly polarized light images. Bone 44, 392-403.

Skedros, J.G., Kiser, C.J., Keenan, K.E., Thomas, S.C., 2011. Analysis of osteon morphotype scoring schemes for interpreting load history: evaluation in the chimpanzee femur. Journal of Anatomy 218, 480-499.

Todoh, M., Tadano, S., Giri, B., Nishimoto, M., 2009. Effect of gradual demineralization on the mineral fraction and mechanical properties of cortical bone. Journal of Biomechanical Science and Engineering 4, 230-238.

Tadano, S., Giri, B., Sato, T., Fujisaki, K., Todoh, M., 2008. Estimating nanoscale deformation in bone by x-ray diffraction imaging method. Journal of Biomechanics 41, 945-952.

Tadano, S., Giri, B., 2011. X-ray diffraction as a promising tool to characterize bone nanocomposites. Science and Technology of Advanced Materials 12, 064708.

Wagermaier, W., Gupta, H.S., Gourrier, A., Roschger, P., Burghammer, M., Fratzl, P., 2006. Spiral twisting of fiber orientation inside bone lamellae. Biointerphases 1, 1-5.

Wang, X.J., Chen, X.B., Hodgson, P.D., Wen, C.E., 2006. Elastic modulus and hardness of cortical and trabecular bovine bone measured by nanoindentation. Transaction of Nonferrous Metals Society of China 16, s744-s748.

Weiner, S., Arad, T., Sabanay, I., Traub, W., 1997. Rotated plywood structure of primary lamellar bone in the rat: orientations of the collagen fibril arrays. Bone 20, 509–514.

Yamada, S., Tadano, S., 2010. Residual stress around the cortical surface in bovine femoral diaphysis. Journal of Biomechanical Engineering 132, 044503.

Yamada, S., Tadano, S., Fujisaki, K., 2011. Residual stress distribution in rabbit limb bones. Journal of Biomechanics 44, 1285-1290.

Figure and table legends

Fig. 1 Schematic representation of the hierarchical structure of bovine cortical bone. In microstructure, the non-osteonal region was defined as the outside area of the osteonal region with lamellar structure.

Fig. 2 The X-ray measurement systems to obtain (a) the HAp crystal strain and (b) the HAp crystal orientation. (a) Collimated X-rays irradiated the specimen face on which a strain gauge glued at the angle θ, and the X-rays diffracted from the (002) lattice plane of HAp crystals aligned to the longitudinal axis of the specimen were detected, to measure the interplanar spacing of the lattice planes and to calculate the HAp crystal strain in tensile tests. The measurement positions were at three points along the longitudinal axis of the specimen. (b) X-rays vertically irradiated the specimen without any external loadings, and X-ray Imaging Plate (IP) detected the X-ray diffraction pattern. The Debye ring of the (002) plane was used to calculate the degree of *c*-axis orientation of HAp crystals in the specimens, because the (002) planes are perpendicular to the *c*-axis of the crystal.

Fig. 3 Microscopic image at the transverse cross-section at the X-ray measurement

position. Osteonal regions were distinguished in the cross-section and the osteon area fraction *OA*, the area ratio of osteonal region to the cross-section area, was calculated. In this image, the *OA* was 0.62.

Fig. 4 (a) Relationship between elastic modulus in the bone axial direction and osteon area fraction $\overline{OA}$. (b) Relationship between tensile strength and $\overline{OA}$.

Fig. 5 Deformation behavior of the HAp crystals in tensile tests. The HAp crystal strain, measured three times at each tissue strain condition and calculated with the displacement of the (002) plane in HAp crystals, was plotted against the applied tissue strain as determined by the strain gauge in the tensile tests.

Fig. 6 Relationship between the degree of *c*-axis orientation of HAp crystals $\langle\cos^2\beta\rangle$ and the osteon area fraction *OA* at the measurement positions.

Fig. 7 Relationship between the elastic modulus and the average of the values of $\langle\cos^2\beta\rangle$.

Fig. 8 Three-dimensional architecture of osteons. A cortical bone specimen of a bovine femur sliced at intervals of about 100 μm and 1 mm-square sections were observed. From the osteonal regions distinguished in these sections, a three-dimensional image was reconstructed and some osteons were extracted in this figure. The result showed that although the osteons bifurcated and converged, osteons were generally aligned with the bone axis.

Figure and table

Figure 1

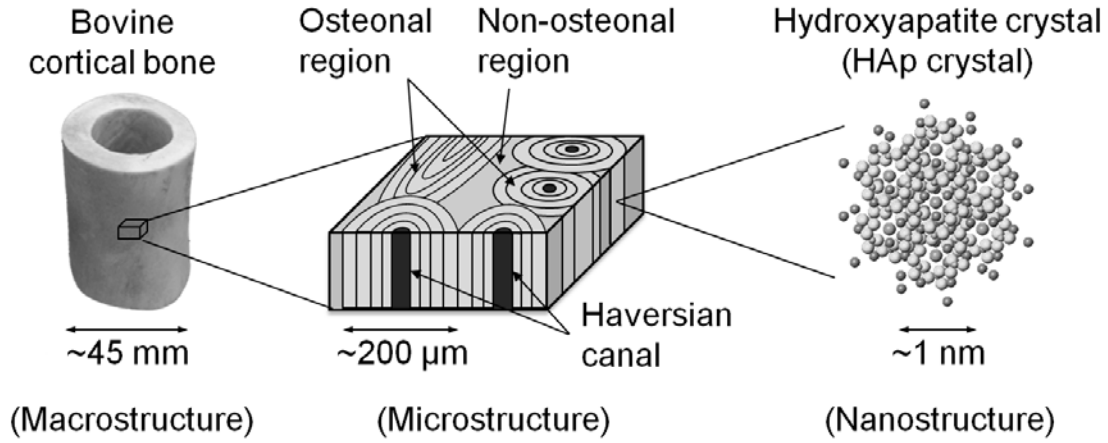

Figure 2(a)

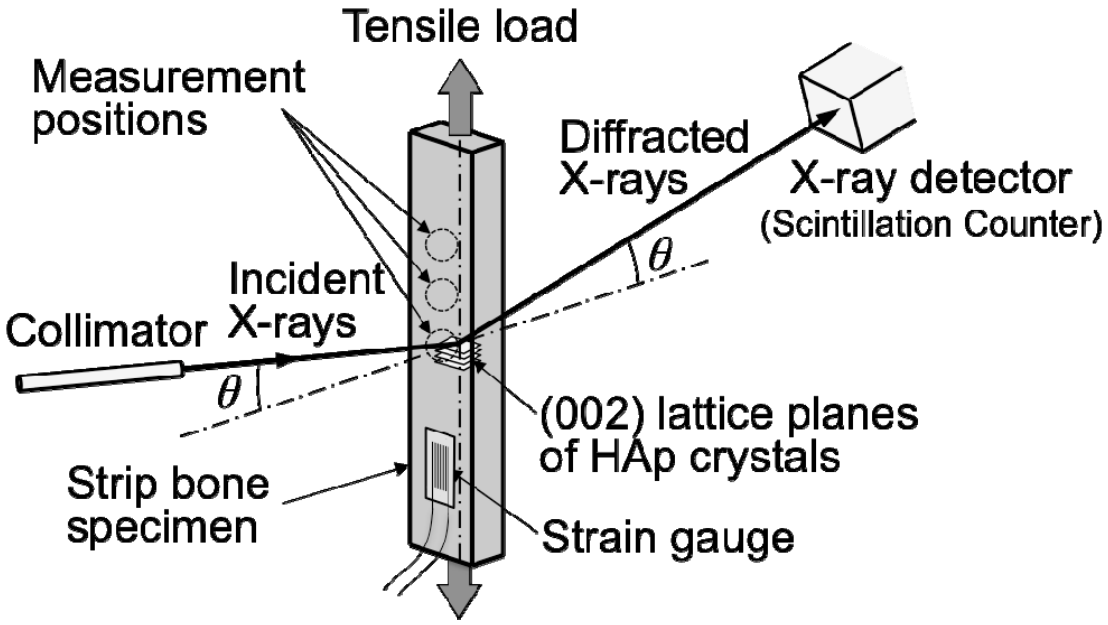

Figure 2(b)

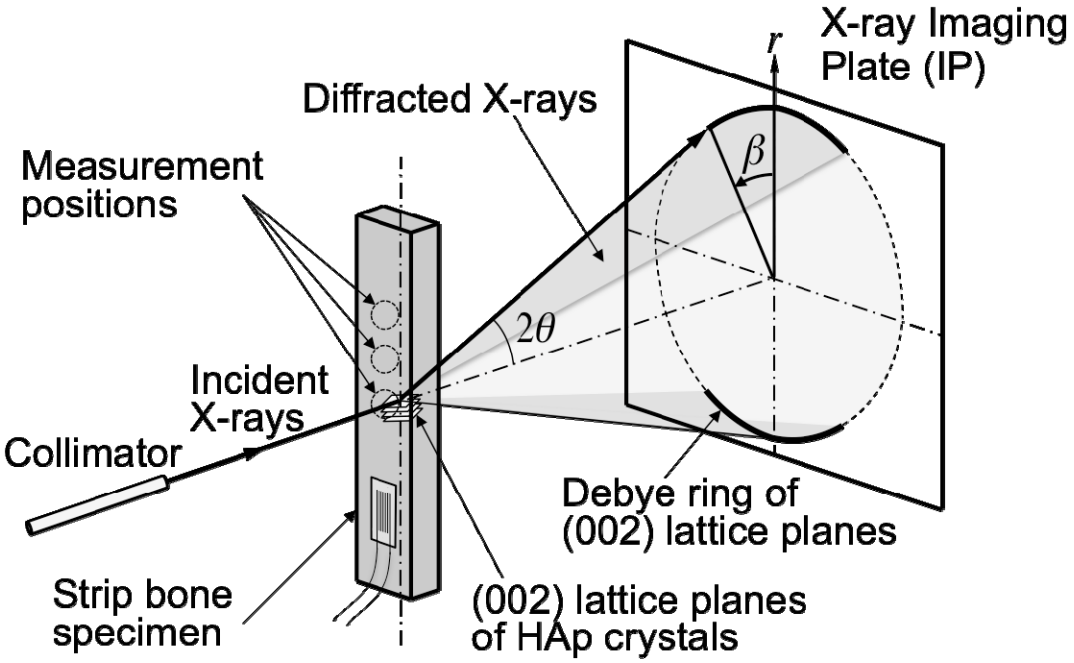

Figure 3

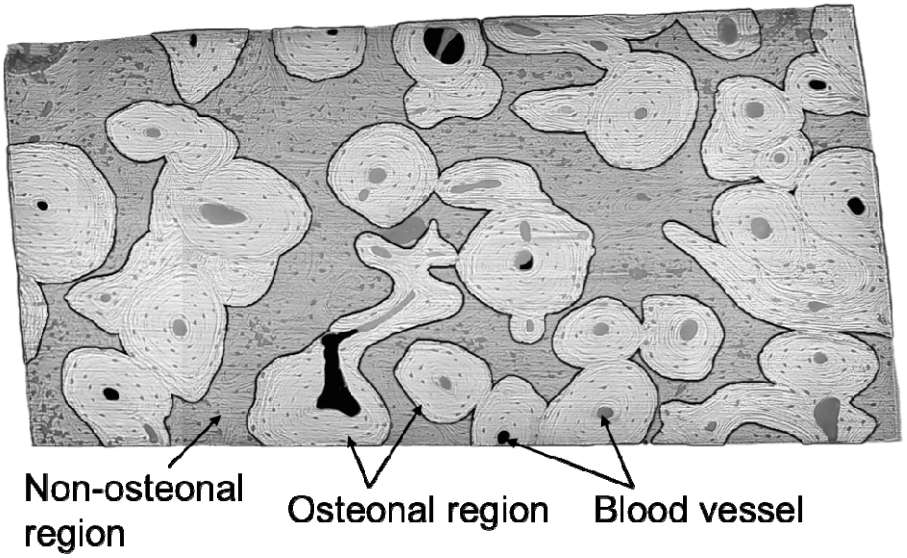

Figure 4(a)

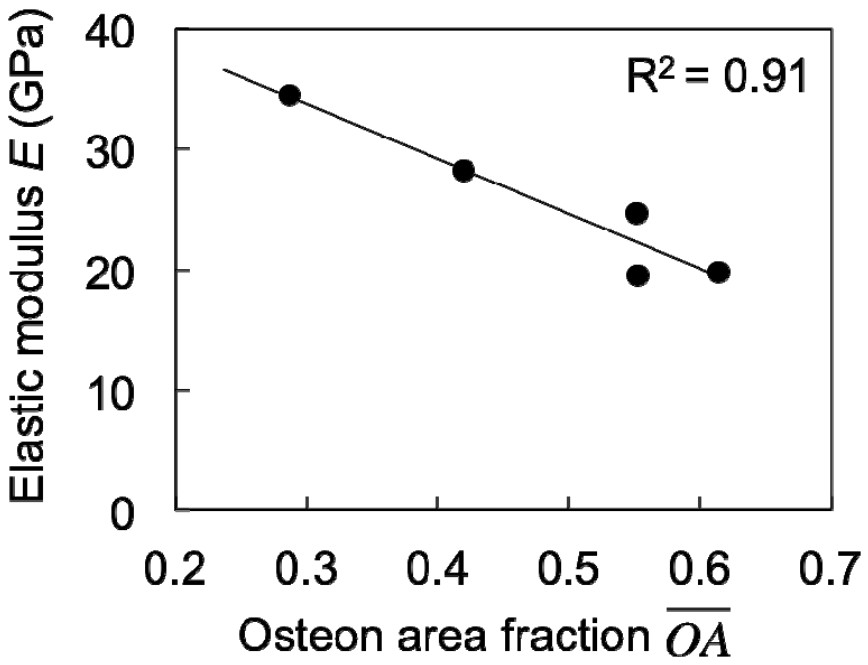

Figure 4(b)

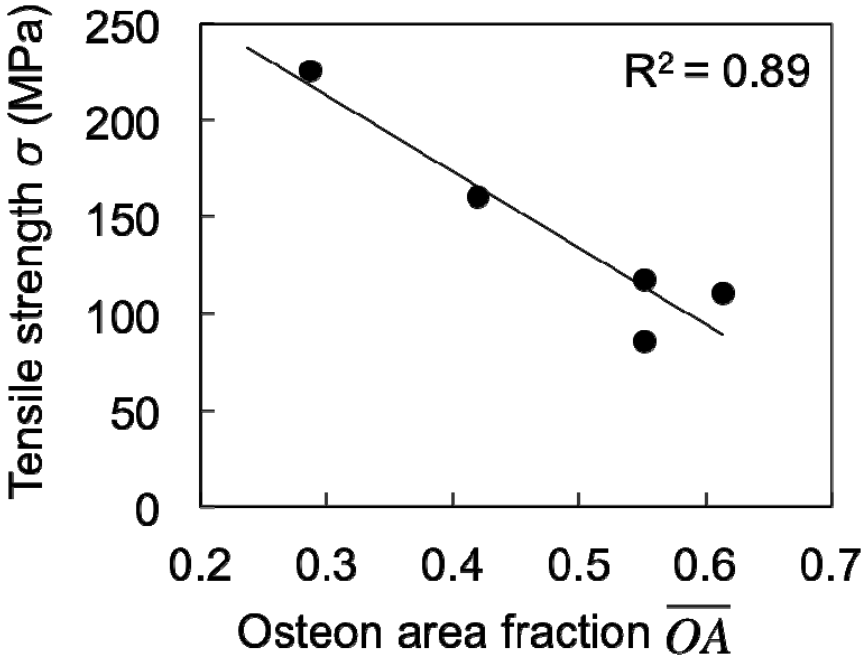

Figure 5

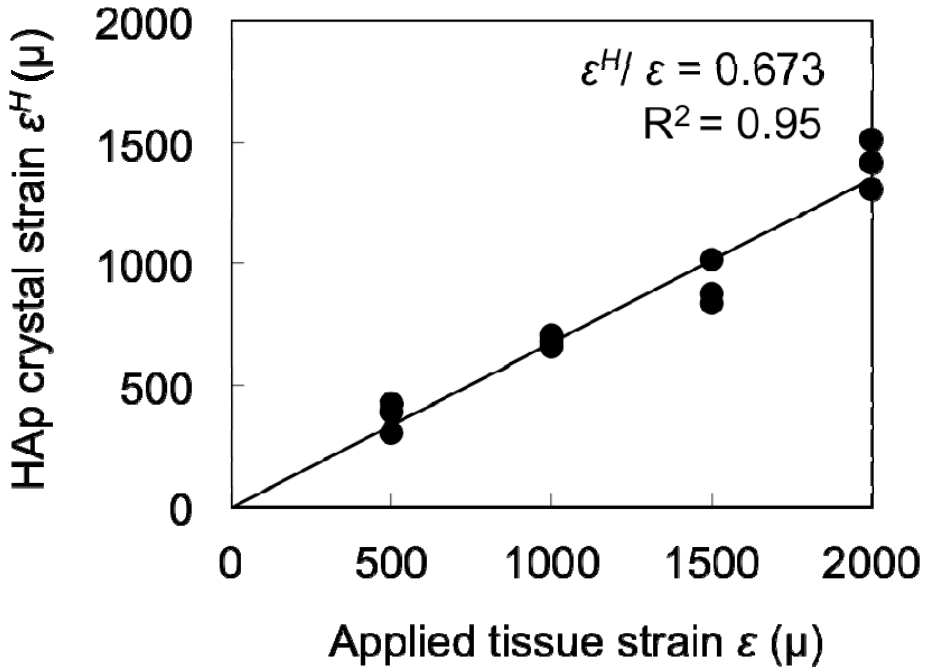
2000
1500
1000
500
0
HAp crystal strain ε^H (μ)
$\varepsilon^H/\ \varepsilon$ = 0.673
R^2 = 0.95
0
500
1000
1500
2000
Applied tissue strain ε (μ)

Figure 6

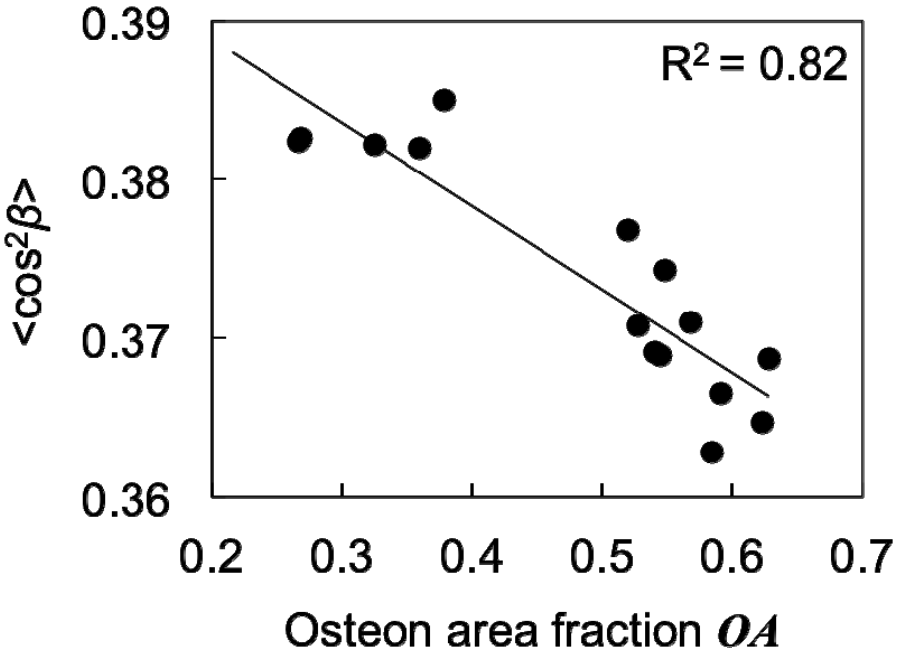
0.39
0.38
0.37
0.36
$R^2 = 0.82$
$\langle \cos^2\beta \rangle$
0.2
0.3
0.4
0.5
0.6
0.7
Osteon area fraction OA

Figure 7

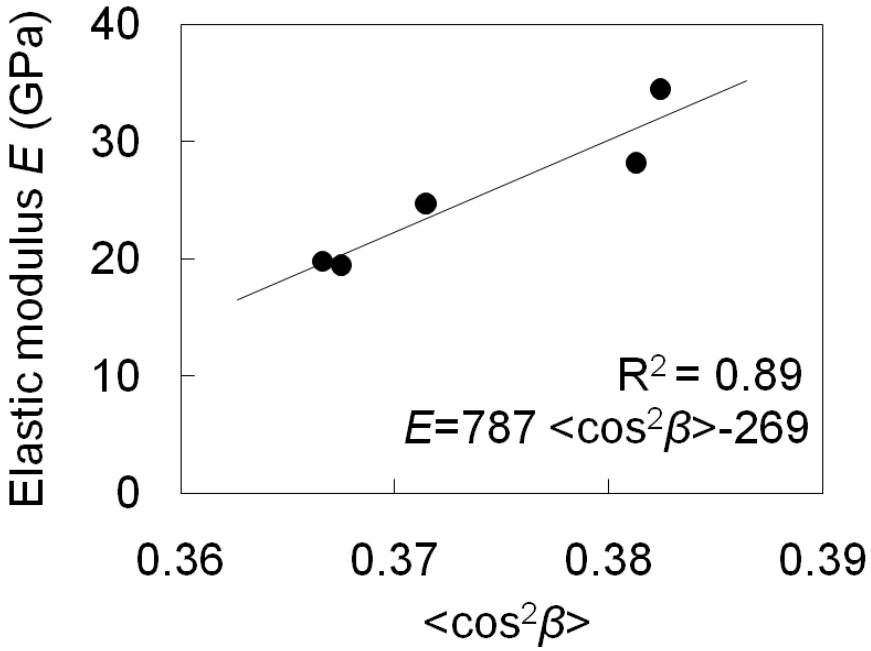
Elastic modulus E (GPa)
40
30
20
10
0
0.36
0.37
0.38
0.39
<cos²β>
R² = 0.89
E=787 <cos²β>-269

Figure 8